Architecture of the MKK6-p38α complex defines the basis of MAPK specificity and activation

Authors: Pauline Juyoux[1]†, Ioannis Galdadas[2, 3]‡, Dorothea Gobbo[2, 3]‡, Jill von Velsen[1], Martin Pelosse[1], Mark Tully[4], Oscar Vadas[5], Francesco Luigi Gervasio[2,3,6,7,8]*, Erika Pellegrini[1]* and Matthew W. Bowler[1]*

Affiliations:

[1] European Molecular Biology Laboratory; Grenoble, France.

[2] Institute of Pharmaceutical Sciences of Western Switzerland, University of Geneva; Geneva, Switzerland

[3] School of Pharmaceutical Sciences, University of Geneva; Geneva, Switzerland.

[4] European Synchrotron Radiation Facility; Grenoble, France.

[5] Protein and peptide purification platform, Faculty of Medicine, University of Geneva, Geneva, Switzerland

[6] Department of Chemistry, University College London; London, United Kingdom

[7] Institute of Structural and Molecular Biology, University College London; London, United Kingdom

[8] Swiss Institute of Bioinformatics, Geneva, Switzerland.

*Corresponding authors. Email: francesco.gervasio@unige.ch, epellegr@embl.fr, mbowler@embl.fr

†Current affiliation: Univ. Grenoble Alpes, CNRS, CEA, IBS, Grenoble F-38000, France.
‡ These authors contributed equally

Abstract

The MAP kinase p38α is a central component of signalling in inflammation and the immune response and is, therefore, an important drug target. Little is known about the molecular mechanism of its activation by double-phosphorylation from MAP2Ks, due to the challenge of trapping a transient and dynamic hetero-kinase complex. We applied a multidisciplinary approach to generate the first structure of p38α in complex with its MAP2K MKK6 and understand the activation mechanism. Integrating cryo-electron microscopy with molecular dynamics simulations, hydrogen-deuterium exchange mass spectrometry, and experiments in cells, we demonstrate a dynamic, multi-step, phosphorylation mechanism, identify catalytically relevant interactions, and show that MAP2K disordered N termini determine pathway specificity. Our work captures a fundamental step of cell signalling: a kinase phosphorylating its downstream target kinase.

One-Sentence Summary: Integrative structure and modelling analysis of an active hetero-kinase complex reveals details of cellular signal transmission.

Mitogen activated protein kinases (MAPKs) are conserved in all eukaryotes where they form signalling cascades responding to extra-cellular stimuli leading to diverse responses from differentiation to apoptosis. In higher organisms, the MAPK p38α acts in response to stress such as irradiation, hypoxia and osmotic shock, and also to signalling from inflammatory cytokines (*1*). Pathogens, including SARS-CoV-2, often elicit upregulation of p38α, which can lead to the cytokine storm associated with severe COVID-19 (*2*, *3*). Signals propagate through phosphorylation of successive protein kinases (MAP4K, MAP3K to MAP2K), which eventually phosphorylate and activate a MAPK via double phosphorylation at the TxY motif in the activation loop (A-loop), leading to a conformational change (*4*, *5*). When the A-loop is phosphorylated, key residues surrounding the ATP and Mg^{2+} ions reorient, stabilising the activated MAPK. The activated MAPK is then transported to the nucleus where it modulates gene expression (*6-8*).

The key role of p38α in inflammation, and the fact that aberrant p38α signalling is implicated in numerous diseases, such as arthritis and cancer, but also in the response to infection, make it a highly studied drug target (*1*). Despite initial successes in developing potent compounds targeting the kinase nucleotide binding pocket, many potential therapies have failed in clinical trials due to off-target effects (*9*). Therefore, a molecular understanding of its interaction with upstream activators is essential in order to develop strategies to target allosteric sites, either in p38 or its activators. The structures of individual MAPKs (*10-12*) and MAP2Ks (*13-16*) have been extensively studied and subsequent work has defined the interacting regions between these partners (*17-20*). The MAP2Ks contain a kinase interaction motif (KIM or D-motif) at the start of their intrinsically disordered N-termini, which interacts with an allosteric docking site on their target MAPK. The KIM partially ensures specificity between members of the pathway (*17*), acts allosterically to expose the A-loop, preparing the MAPK for activation (*21*, *22*), and also enhances the local concentration of kinase and substrate (*23*). However, there is little structural data on the global interactions between MAP kinase cascade components. Beyond the KIM interaction, molecular details of selectivity and activation of a MAPK by its upstream MAP2K remain unknown. Moreover, our knowledge of kinase-kinase interactions, in general, is restricted to homodimers and inactive conformations (*24-29*).

In order to further our understanding of how signals are transmitted through the MAP kinase pathway, we applied a multi-disciplinary approach, combining cryogenic electron microscopy (cryo-EM) with hydrogen-deuterium exchange mass spectrometry (HDX-MS), small angle X-ray scattering (SAXS), enhanced sampling molecular dynamics (MD) simulations and cellular assays, to characterise a complex between the MAP kinase p38α (MAPK14) and its activating MAP2K MKK6 (MAP2K6). Here, we present a detailed molecular model of this highly dynamic and transient interaction between signalling components, providing insights into specificity and multi-step catalysis. Our findings open routes to drug development for the important MAPK signalling pathway and lead to a better understanding of a crucial step in kinase signalling cascades.

Engineering an active and stable MKK6-p38α complex for structural studies

The MAP kinases are malleable proteins that must adapt to multiple upstream and downstream effectors, as well as phosphorylate a large range of substrates. The proteins therefore adopt multiple conformations, and interactions with effectors and substrates must be transient in order to maintain signal transmission. To stabilise the MKK6-p38α complex for structural studies, we created a chimera of MKK6, named MKK6^{DD}GRA, where we replaced the native KIM with that from the *Toxoplasma gondii* effector protein GRA24 (*30*) that has a 100-fold higher affinity for p38α, but induces the same conformation as the MKK6 KIM (Fig. S1A) (*31*). We also inserted phosphomimetic mutations in the MKK6 A-loop (S207D and T211D) to transform the kinase into a constitutively active form, ready to phosphorylate p38α (Fig. 1A and S1B and C). Analysis by SAXS revealed heterogeneity in the size of the complex formed with p38α (Fig. S2A). By screening MKK6^{DD}GRA with a combination of different nucleotide analogues and p38α A-loop mutants, we identified the mutant p38α^{T180V} (one of the phosphosites of the A-loop) in combination with the transition state analogue ADP.AlF_4^- as the complex with the smallest radius of gyration (Rg) (Table S1). As a smaller Rg for a given sample indicates a more compact structure, we reasoned that in this sample, the transition state analogue complex is stably assembled with the single residue available in the A-loop (Y182) and should be suitable for structural studies. Subsequent analysis, including HDX-MS, MD, and Bayesian modelling confirmed that the engineering increases the population of the transphosphorylation-competent state of the complex and that its nature is consistent with that of the wild type (see below).

Architecture of the MKK6-p38α complex

We imaged the 80 kDa MKK6^{DD}GRA-p38α^{T180V} complex by cryo-EM (Fig. 1). The purified complex was well dispersed and yielded 2D class averages that showed clear secondary structure features (Fig. 1B). The selected particles allowed the 3D reconstruction to a nominal resolution of 4 Å (map range 2.7-6.5 Å, Fig. 1C and S3, Movie S1). The final resolution was limited not only by the small size of the complex, but also by the highly dynamic nature of the interaction between the kinases, leading to particle heterogeneity. Therefore, very strict selection of particles was necessary to capture this conformation. Multiple rounds of picking and retraining using Topaz (*32*) led to a good quality set of particles that could then be further selected in 2D classification to remove particles clearly showing only a single kinase or two loosely connected kinases (these classes were always low resolution). Subsequent rounds of heterogeneous refinement and quality assessment via 2D classification were then used to differentiate between face-to-face conformations where the A-loop was stabilised or disordered.

To build the model of the complex, we docked structures of p38α and MKK6 into the map. As all structures of inactive p38α available have an unstructured or mobile A-loop, we determined

the crystal structures of human p38α, and an inactive mutant (p38α^{K53R}), in which the A-loops are well ordered, in the occluded conformation, in order to have a starting point for refinement of the extended conformation (Table S2). The available MKK6 structures are not in the active conformation (Fig. S4). We therefore modelled the structure from the active conformation of MKK7 (*16*). Docking of these structures was followed by one round of morphing and real space refinement. We then computed the cross-correlation between experimental and predicted maps for relevant structures obtained from the ensemble obtained by combining Bayesian inference with MD simulations and SAXS data to select the model that best recapitulates the available data (Fig. 1D and S3C, Tables S3 and S4). The reconstruction shows the kinases adopting a 'face-to-face' conformation with most contact between the C-lobes. MKK6 is in the active kinase conformation based on its αC-helix rotated position and the DFG-in BLA- conformation according to kinase nomenclature (*33*) (Fig. S4), and density can be observed for nucleotide in its active site (Fig. S5). The p38α A-loop is ordered and extends toward the MKK6 active site; however, it remains dynamic, limiting the resolution of this region (Fig. S5). The p38α active site also binds nucleotide (Fig. S5), implying it is already in an active conformation. MKK6 interacts with the p38α CD site through the GRA24 KIM at the start of its N-terminal extension, which can be traced in the density (Fig. 1C and S5). Most of the linker between the KIM and the MKK6 kinase core, as well as the MKK6 A-loop, remains disordered and, therefore, unresolved. Interestingly, AlphaFold2 multimer (*34*) predicts a similar face-to-face conformation for the MKK6-p38α^{WT} complex, as well as for MKK6^{DD}-p38α^{WT} and MKK6^{DD}GRA-p38α^{T180V} (Fig. S6). Superimposing the predicted models to our experimental model shows a high consensus of the interaction. However, relative domain rotation in the prediction leads to differences in the interface of the two kinases (Fig. S6A). High confidence in intermolecular contact placement seen in the predicted aligned error (PAE) plots (Fig. S6D to F) support the overall face-to-face conformation of the complex.

The main kinase core fold interaction is between the αG-helix (residues 262-273) of MKK6 and a hydrophobic pocket in p38α, partly formed by the MAPK-specific insert in the C-lobe (Fig. 2A, C and D, Movie S2), that clamps the MKK6 αG-helix upon binding (Movie S3). This insert has been described as a lipid-binding site important in regulation (*35*, *36*) and several studies have identified small molecules that target this pocket (*37-41*) (Fig. S7). This site has also been shown to be important in MAPK substrate binding (*42*, *43*) (Fig. S7). The exposed residues of this helix, as well as residues lining the MAPK hydrophobic pocket, are highly conserved in the MAP2Ks and MAPKs, respectively, suggesting a common interaction site for the pathways (Fig. 2E). Additionally, there is a potential interaction between the N-lobes via the loop between the β3-sheet and αC-helix of MKK6 (residues 87-89) and β-strands 1, 2 and 3 of the N-lobe of p38α (Fig. 2B). We validated the observed interactions using HDX-MS (*44*). In both the MKK6^{DD} (with the wild type KIM) and chimera MKK6^{DD}GRA, several regions were protected from hydrogen/deuterium exchange in the presence of an excess of p38α: the N-terminus, the β3-strand, the A-loop and the αG-helix (Fig. 2G and S8 and Table S5). The interaction sites identified in solution highly correlate with the cryo-EM model for both the wild type and chimeric complexes. Although no peptide was detected for MKK6 KIM, the GRA24 KIM was strongly protected upon binding with p38α. In an excess of MKK6^{DD} only the p38α MAPK insert and a small region of the N-lobe are protected from exchange (Fig. 2G and S8). We also evaluated the protection on p38α when we mutated the MKK6 αG-helix residues facing the p38α hydrophobic pocket to alanine (F264A, Q265A, L267A, K268A, E272A – referred to as MKK6^{DD} αG-helix mutant). Unlike with MKK6^{DD}, the p38α MAPK insert is not protected in the presence of the MKK6^{DD} αG-helix mutant, which implies that this mutant cannot interact with p38α in that region (Fig. S9). Free energy calculations of p38α-MKK6 and p38α-MKK6 αG-helix mutant further support the lower stability of the C-lobe interface in the latter ("Additional text" in the Supporting Information and Fig. S9). These experiments

define the αG-helix – MAPK insert interaction as the primary site of interaction between the two kinases during phosphorylation of the p38α A-loop.

To further study the importance of these interactions on p38α activation, we used the MKK6^{DD} αG-helix mutant and also mutated the β3-αC loop of the MKK6 N-terminal interaction to alanine residues (T87A, V88A, N89A – referred to as MKK6^{DD} β3-αC loop mutant) and read out the effect on p38α signalling in cells using a reporter luciferase assay (Fig. 2F). We transiently transfected HEK293T cells with p38α and MKK6^{DD} mutants, together with a plasmid encoding firefly luciferase under the control of the AP-1 promoter, where AP-1 activity is stimulated by p38α via several substrates (e.g. ATF2, see Materials and Methods). The MKK6^{DD} αG-helix mutant reduced p38α signalling by 70% when compared to MKK6^{DD}, demonstrating the important role this interaction plays in p38α activation. The MKK6^{DD} β3-αC loop mutant increased signalling to ~170% over MKK6^{DD}. This loop is the site of numerous activating mutations, particularly in cancer, that stabilise the 'αC-in' conformation (*45*, *46*). This could explain the observed increase in signalling but does not rule out a role of the p38α N-lobe in the stabilization of the active conformation of MKK6 in the face-to-face complex.

Molecular dynamics confirm the complex is metastable and show how catalytically competent states can be formed

To better understand the details of the heterogeneous structural ensemble of the complex, and the mechanism of transphosphorylation of p38α on T180 and Y182 by MKK6, we ran a series of MD simulations, starting with a set of 18 simulations, each 1 μs long (Table S7). The simulations started from models derived from the cryo-EM structure: MKK6GRA-p38α (with WT A-loop) and MKK6-p38α, where we reverted the GRA24 KIM back to the WT sequence.

The simulations explored several conformations. In most cases, the contact between the KIM and p38α was retained, and catalytically competent states, where p38α T180 or Y182 approached the γ-phosphate of MKK6 ATP at a catalytically compatible distance, were observed. Partial detachment of p38α from MKK6 was also observed in some instances. Additionally, the C-lobe interface proved to be important for the stability of the dimer, in agreement with our other observations. In all simulations in which the two kinases break apart, this tight hydrogen-bonding network at the C-lobe level is the last point of contact to be lost. In particular, the interaction between MKK6 αG-helix residues K268 and E272 and p38α S261 seems to be one of the main interactions keeping the two kinases in close proximity (Fig. S9E). The observed conformational variety is consistent with the SAXS and cryo-EM data, which are indicative of the transient nature of the interaction of the two kinases. With respect to the phosphorylation mechanism, in a number of trajectories, either p38α T180 or Y182 approach the ATP γ-phosphate located in the MKK6 active site (*47*) (Fig. 3 and Table S8, Movies S4 and S5). In particular, in the simulations of MKK6-p38α, both T180 and Y182 come close to the catalytic site. The tendency of monomeric, unphosphorylated p38α to adopt inactive, sequestered, A-loop conformations has been shown in previous studies (*48*). Thus, the observation that the unphosphorylated A-loop of p38α adopts an exposed conformation in multiple instances is indicative of an active role of MKK6 in stabilizing such conformations. The active role of MKK6 is confirmed by the fact that in the simulations in which the MKK6 KIM detaches, leading to the separation of the two kinases, the p38α A-loop transitions from an exposed to a sequestered conformation (Fig. S11).

A rotated complex might facilitate the phosphorylation of p38α T180

In this initial set of MKK6GRA-p38α simulations, we observe some complexes in which T180 approaches the γ-phosphate of ATP in the catalytic site of MKK6 from an unexpected angle, where the p38α N-lobe underwent a 50-80° rotation around its axis (Fig. 3B, Movie S4). In this conformation, p38α was kept close to MKK6 through the KIM, despite the rotation. Before T180 gets close to the ATP, a key lysine located just after the KIM, K17, forms a salt-bridge with p38α E160 which seems to initiate the rotation of p38α (Fig. 3C).

Integration of simulations with SAXS data using Bayesian/Maximum entropy reweighting shows how the kinases associate

To better characterize intermediate states involved in the formation of the catalytically competent dimer, we extended the conformational sampling of the MD simulations using adaptive Markov state model (MSM) simulations (*49, 50*) (details in SI) and used a kinetic-based clustering of the total accumulated MD trajectories to determine the main metastable states. By extending the sampling to more than 18 μs and performing the kinetic clustering, we obtain five macro-states for p38α with MKK6GRA (Fig. 4 and Movies S6-S10). In the case of MKK6GRA-p38α, one of the clusters corresponds to an ensemble which contains conformations where the two kinases are face-to-face, equivalent to the cryo-EM structure (state A, Movie S6). Interestingly, in this macro-state, we also see conformations corresponding to the rotated N-lobe of p38α, in which T180 is ideally positioned for phosphorylation. The fact that the face-to-face and rotated conformations cluster within the same metastable state reflects the rapid interconversion from one to the other (few μs). In the second macro-state, the KIM is tightly bound, whereas MKK6 adopts different orientations (state E, Movie S7). The third macro-state represents conformations resulting from the detachment and non-specific binding of the two kinases, in which MKK6 binds to different surfaces of p38α (state C, Movie S8). Finally, we observe two macro-states in which the two kinases are held together through the C-lobe interface and in which the KIM is either bound (state B, Movie S9) or explores the N-lobe of p38α (state D, Movie S10). The connections between the macro-states (Fig. 4) indicate one or more reactive trajectories connecting one state to another. The resulting network shows that the binding of the KIM to its recognition site plays a fundamental role in establishing the specific contacts needed for the formation of the face-to-face dimer.

Despite a total sampling time of more than 18 μs, we could not fully converge the kinetics and the population of all the macro-states directly from the simulations, probably due to the slow nature of some of the transitions seen in protein-protein associations (*50*). An exhaustive sampling of complex formation from the detached states would require a prohibitive number of long MD simulations and might still be affected by the quality of the force field. We therefore refined the structural ensemble and validated the clustering results by using the SAXS data and a Bayesian/maximum entropy approach (*51-53*). The SAXS profile of each conformer within the clustered MD ensemble was calculated, and the weights associated with each conformer in the ensemble that maximise the agreement with experiments were iteratively determined (Fig. S12A). For the refinement of the MKK6GRA-p38α ensemble, we used the SAXS curves of the complex with ADP.AlF_4^- and with the non-hydrolysable ATP analogue AMP-PCP. The reweighted ensemble fits extremely well with the SAXS curve of $MKK6^{DD}$GRA-$p38\alpha^{T180V}$ with ADP.AlF_4^- (χ^2=0.89, Movie S15), which showed the most compact conformation (Table S1). Reassuringly, all the macro-states from kinetic modelling contribute to it (Fig. 4). State A, which contains conformations equivalent to the cryo-EM structure, is the most populated (62.5%), followed by state C (27.8%), which reflects the transient nature of the complex and the non-specific binding associated with such transient complexes, and finally ensemble E (2.5%). From the weights (and

the other experiments), we deduce that the latter is the main intermediate for the formation of the face-to-face complex. After the KIM domain is bound, the MD simulations indicate an important role for the hydrophobic patch and a network of hydrogen bonds located at the interface of the C-lobes of the two kinases in the formation of the complex. These conclusions are in accordance with the 70% decrease in activity seen in the $MKK6^{DD}$ αG-helix mutant (Fig. 2F), as well as the metadynamics free energy calculations and the HDX-MS data (Fig. S9).

The ensemble reweighted to match the SAXS data obtained with the $MKK6^{DD}$GRA-$p38\alpha^{WT}$ with the ATP analogue AMP-PCP also resulted in a good fit (χ^2=2.1). The population of the face-to-face cluster A decreases to 1% whereas that of the detached cluster C and intermediate D increases considerably, to 71.5% and 21.7%, respectively (Fig. S12B, C). Although the populations of the macro-states shift, as expected as the transition state is not stabilised, the general description of the macro-states remains similar. Within cluster A, the weights of the 'rotated' face-to-face dimer increase (Fig. S12B). We also sampled the conformational space of the MKK6-p38α with the same adaptive MSM approach. The four macro-states found in the MKK6-p38α complex are equivalent to four of the macro-states found in MKK6GRA-p38α (Fig. S13), reflecting the similarity of the dynamics of the two complexes (see Supplementary text).

The N-terminal extension of MKK6 remains mainly disordered and its length and secondary structure elements contribute to pathway specificity

Our structure and macro-state modelling imply that once the KIM is bound the N-terminal linker plays an important role in conformational sampling, allowing the catalytically competent state to form, a phenomenon that has been observed in other tethering proteins (*54*). There is a wealth of data on interactions between KIMs and MAPKs, but the role of the remainder of the N-terminus is poorly understood (*55, 56*). In our cryo-EM map, the engineered KIM is clearly visible (Fig. 1C and S5), but it does not appear to interact further with p38α. To investigate whether the N-terminal extension has a role beyond simply associating the kinase to the KIM, we again used the luciferase reporter assay. We produced constructs that scan the region between the KIM and the first consensus β-sheet of the kinase core with alanine blocks in order to determine if there is sequence specificity or direct interaction with p38α (Fig. 5). Our results show that the sequence of the middle region ($MKK6^{DD}$ Ala scan 28-39) of the N-terminal linker has no effect on p38α signalling *in cellulo*. However, the sequence of the linker close to the KIM ($MKK6^{DD}$ Ala scan 18-29) and the region close to the kinase core, which comprises the predicted β-strands ($MKK6^{DD}$ Ala scan 38-49, Fig. 5) seem to have some importance as their mutation to alanine reduced p38α signalling by 27% and 58% respectively.

Although KIM sequences are important, they do not sufficiently explain specificity. Comparing the N-terminal linkers of the MAP2Ks, they differ in their length and secondary structure elements (*16, 57, 58*) (Fig. 5B and C). Could this contribute to specificity between the pathways? When we substituted the MKK6 linker with those from the MAP2Ks of the other pathways, activity was reduced (Fig. 5D). This is most drastically observed with the linkers from MEK1 and 2. Even the linkers from MAP2Ks that activate p38α see reduced activity and are not sufficient to rescue the activation, even though the KIM, MAP2K and MAPK are in the correct combination. Our structure and macro-state models imply that the length of the linker is just sufficient to allow the observed interactions between the kinases, in particular, the MAP2K αG-helix position relative to the MAPK hydrophobic pocket formed by the MAPK insert. By removing or adding 10 residues to the linker region, activity is reduced by ~50%. This implies that the length of the linker, controlled by either the number of amino acids and/or secondary structure elements, is important in the positioning of the MAP2K for engagement with the MAPK and is finely tuned

for MAP kinase pairs. The specificity of a MAP2K is therefore defined by cooperation between the KIM, the linker, and the kinase core folds themselves.

Discussion

Initial docking

The N-termini of the MAP2Ks contain a conserved KIM motif that is required for binding to their substrate MAPKs. The first step in activation is KIM binding after which a wide variety of conformations are observed, showing the fast timescale of association/dissociation. During the MD simulations, KIM binding induced allosteric changes in p38α, which adopts a prone-to-be-phosphorylated conformation with its A-loop extended, exposing the tyrosine and threonine residues, in agreement with crystal structures. Our data indicate that the interaction between the MKK6 N-terminus and p38α extends beyond the hydrophobic residues of the KIM and is important in the activation process. Although most of the MKK6 N-terminal linker remains disordered, its length seems to be tightly linked to the substrate MAPK and the presence of some secondary structural elements differs between MAP2Ks contributing to specificity (Fig. 5C). Our reweighted ensemble, obtained by combining Bayesian inference with adaptive MSM simulations and SAXS data, shows that once the KIM is bound, many conformations are sampled before the engagement of the αG-helix (Fig. 4). This sampling is fully consistent with the experiments that show that if the linker is not the correct length, the engagement of the αG-helix will be impeded. Once p38α is recruited, some parts of the MKK6 N-terminal linker could participate in the conformational shift towards the MKK6 active conformation, but its main function appears to be to prepare the MAPK A-loop and guide the engagement with the αG-helix.

Engagement with substrate

We show that the predominant interaction during activation is mediated by the αG-helix of the MAP2K MKK6 and the p38α hydrophobic pocket formed by the αG-helix of p38α and the specific MAPK insert. This region is also important in MAPKs for substrate recognition (*42*) and interaction with scaffold proteins and downstream regulators such as phosphatases (*27, 43, 59*). The engagement of αG-helices seems to be an emerging theme in kinase heterodimers: only a few structures have been determined, such as the KSR2-MEK1 heterodimer (*27*) and more recently, the BRAF-MEK1 complex (*25*), both upstream components of the related ERK MAPK pathway. In both these structures the αG-helices interaction is very similar, as well as the relative orientation of the kinases. Several studies have shown that small molecules can target this region in p38 isoforms (*37-41*) and modulate the position of the MAPK insert helices (Fig. S7). However, as the pocket is very deep, the molecules may not extend far enough to disrupt the interactions identified here. There has been intense interest, and some success (*60*), in developing drugs that target p38α, mostly binding to the nucleotide pocket, but they have been mired by off-target and toxicity effects (*9*). The molecules that have been identified as binding to the MAPK insert pocket could be further developed to better disrupt both the MAP2K interaction, and that of substrates, which could lead to highly specific p38 inhibitors.

The MKK6 KIM–p38α docking site, the MKK6 N-terminal linker, and the MKK6 αG-helix–p38α hydrophobic pocket interactions, are clearly essential for defining the specificity of the kinase-substrate interaction, for positioning the two kinases, and for triggering the necessary changes towards the MKK6 active kinase conformation and positioning the A-loop of p38α to be accessible for phosphorylation. Our data demonstrate that altering any of these three components perturbs the activation of downstream signalling.

Freedom of interaction at the catalytic centre

All contacts observed between the kinases are distal to the active site, explaining the lack of sequence specificity or conservation in MAPK A-loops in the region preceding the TxY motif (*58*) and our HDX-MS data show no tight interaction between the A-loop of p38α and MKK6 (Fig. 2 and S8). Rather than the active site of a classical enzyme, where substrates are perfectly positioned for catalysis, the MAP2K-MAPK complex appears to provide a zone of proximity, allowing the flexible activation loop to move, but increasing the probability, or local concentration, of the p38α T180 and Y182 residues to be positioned for nucleophilic attack of the γ-phosphate of ATP by relative positioning of the two kinases. Dual specificity MAP2Ks are unusual as the two amino acids targeted are significantly different to each other, when compared to serine/threonine kinases. In addition, the two substrate phosphorylation sites are only one residue apart and the MAP2Ks need to have an active site that can accommodate, effectively, four substrates (A-loop **T**-x-Y; T-x-**Y**; **T**-x-Y^P; T^P-x-**Y** (targeted residue in **bold**)), all with significantly different sizes and charges. This implies that flexibility in the active site is essential to accommodate such a wide variety of substrates. By not binding any residues of the A-loop specifically, various residues and phosphorylation states could be accommodated by sacrificing catalytic efficiency for flexibility.

The MD simulations revealed that the face-to-face architecture of the hetero-kinase dimer of our model is compatible with the phosphorylation of either T180 or Y182 of the p38α A-loop (Fig. 3 and S14). Another conformation, where p38α rotated, emerged and seems to favour the phosphorylation of T180. Kinetic data have shown that the dual phosphorylation of p38α by MKK6 involves a partially processive mechanism *in vitro*, in which the monophosphorylated intermediates can either dissociate from the enzyme or proceed to the next catalytic step. Wang *et al. (61)* and others (*62*) propose that both p38α monophosphorylated forms can be produced by MKK6 catalysis with a preference for Y182, whose phosphorylation is four-fold faster than that of T180. With respect to the second catalytic step, the experimentally measured kinetic rates indicate that phosphorylation at Y182 in the first step enhances the catalytic efficiency of MKK6 phosphorylation at T180 in the second step. According to our simulations (Fig. 3 and S14), when the N-lobe of p38α undergoes a large conformational change towards the rotated dimer, T180 is in the right position to be phosphorylated, but Y182 is more distant from the catalytic site, which might explain the observed lower catalytic efficiency of MKK6 when the second phosphorylation is on Y182 by kinetic measurements. Conversely, Y182 seems to be able to easily approach MKK6 ATP in the face-to-face catalytically-competent conformations and then be phosphorylated. Thus, the difference in the experimental kinetic rates measured for the first phosphorylation step may reflect the rotation of the p38α N-lobe around its axis, which seems to be involved in the T180 phosphorylation only. The partial processivity of the dual phosphorylation in a cellular context remains an open question (*63, 64*), but the architecture of the interaction we observe between MKK6 and p38α, as well as the micro-states seen in modelling seems to be compatible with either a distributive, partially processive or fully processive mechanism.

By combining cryo-EM and MD simulations, together with HDX-MS and structure-driven mutagenesis *in cellulo*, we describe the range of attributes that lead to MKK6 selectivity and p38α activation. Moreover, we identify critical interfaces for dimer stabilisation. In this regard, small molecules that prevent MKK6-p38α complex dimerization could be therapeutically effective in treating diseases resulting from abnormal MKK6-p38α-mediated signalling. What is more, our data describe molecular details of the activation of one protein kinase by another – one of the most fundamental mechanisms in cell signalling.

Materials and Methods Summary

The details of the methodology are described in the supplementary materials and are summarized here as follows:

Purification of MKK6-p38α complexes

Human MAPK p38α constructs were expressed in *E.coli* with an N-terminal His6 tag and purified via nickel affinity and size exclusion chromatography. To increase the affinity of the constitutively active $MKK6^{DD}$ mutant (S207D and T211D) for p38α for structural studies, the natural KIM sequence was replaced with the *T. gondii* effector protein GRA24 KIM sequence ($MKK6^{DD}$GRA) and a C-terminal Twin-Strep tag added. $MKK6^{DD}$ and $MKK6^{DD}$GRA were expressed in *Sf21* insect cells and purified via streptavidin affinity and size exclusion chromatography. The hetero-kinase complex was prepared by mixing $MKK6^{DD}$GRA and p38α in a 1:1 molar ratio followed by size exclusion chromatography. The transphosphorylation conformation was then assembled using the transition state analogue $ADP.AlF_4^-$ by incubation with 10 mM ADP, 10 mM NH_4F and 1 mM $AlCl_3$ for 30 minutes before proceeding with biophysical studies.

Cryo-EM grid preparation, imaging, data processing and modelling

Purified $MKK6^{DD}$GRA-$p38\alpha^{T180V}$ with $ADP.AlF_4^-$ was applied to UltraAufoil 1.2/1.3 grids and plunge-cooled using a Vitrobot Mark IV (FEI), screened on a FEI Talos Glacios (EMBL Grenoble) and imaged on a FEI Titan Krios (EMBL Heidelberg). Data processing yielded a final map with an average resolution of 4.0 Å resolution (FSC 0.143) showing the two kinases in a face-to-face conformation with the A-loop of p38α extended towards the active site of MKK6.

MD simulations and modelling

The cryo-EM structure was used as the starting conformation of the MD simulations and bound nucleotides were replaced with ATP. The simulations were set up using GROMACS v.2021.3 with the DES-Amber force field and TIP4PD water molecules. The PLUMED plugin was used for free energy calculations. Adaptive MD simulations were performed to further explore the prebound and bound states of the complex. The conformational ensembles were clustered kinetically and refined using an iterative Bayesian/Maximum Entropy (iBME) protocol to obtain a structural ensemble that reflects the states captured in the solution SAXS data.

References and Notes

1. B. Canovas, A. R. Nebreda. "Diversity and versatility of p38 kinase signalling in health and disease", *Nat Rev Mol Cell Biol* **22**, 346 (2021).10.1038/s41580-020-00322-w
2. M. Bouhaddou *et al.* "The Global Phosphorylation Landscape of SARS-CoV-2 Infection", *Cell* **182**, 685 (2020).10.1016/j.cell.2020.06.034
3. Daniella S. Battagello *et al.* "Unpuzzling COVID-19: tissue-related signaling pathways associated with SARS-CoV-2 infection and transmission", *Clinical Science* **134**, 2137 (2020).10.1042/cs20200904
4. S. Bellon, M. J. Fitzgibbon, T. Fox, H.-M. Hsiao, K. P. Wilson. "The structure of phosphorylated P38γ is monomeric and reveals a conserved activation-loop conformation", *Structure* **7**, 1057 (1999).https://doi.org/10.1016/S0969-2126(99)80173-7
5. S. S. Taylor, A. P. Kornev. "Protein kinases: evolution of dynamic regulatory proteins", *Trends in Biochemical Sciences* **36**, 65 (2011).https://doi.org/10.1016/j.tibs.2010.09.006

6. N. Bluthgen *et al.* "Effects of sequestration on signal transduction cascades", *FEBS J* **273**, 895 (2006).10.1111/j.1742-4658.2006.05105.x
7. F. Ortega, L. Acerenza, H. V. Westerhoff, F. Mas, M. Cascante. "Product dependence and bifunctionality compromise the ultrasensitivity of signal transduction cascades", *Proc Natl Acad Sci U S A* **99**, 1170 (2002).10.1073/pnas.022267399
8. M. Thattai, A. van Oudenaarden. "Attenuation of noise in ultrasensitive signaling cascades", *Biophys J* **82**, 2943 (2002).10.1016/S0006-3495(02)75635-X
9. D. Hammaker, G. S. Firestein. "“Go upstream, young man”: lessons learned from the p38 saga", *Annals of the Rheumatic Diseases* **69**, i77 (2010).10.1136/ard.2009.119479
10. K. P. Wilson *et al.* "Crystal structure of p38 mitogen-activated protein kinase", *J Biol Chem* **271**, 27696 (1996).10.1074/jbc.271.44.27696
11. X. Xie *et al.* "Crystal structure of JNK3: a kinase implicated in neuronal apoptosis", *Structure* **6**, 983 (1998).10.1016/S0969-2126(98)00100-2
12. F. Zhang, A. Strand, D. Robbins, M. H. Cobb, E. J. Goldsmith. "Atomic structure of the MAP kinase ERK2 at 2.3 Å resolution", *Nature* **367**, 704 (1994).10.1038/367704a0
13. X. Min *et al.* "The structure of the MAP2K MEK6 reveals an autoinhibitory dimer", *Structure* **17**, 96 (2009).10.1016/j.str.2008.11.007
14. T. Matsumoto *et al.* "Crystal structure of non-phosphorylated MAP2K6 in a putative auto-inhibition state", *J Biochem* **151**, 541 (2012).10.1093/jb/mvs023
15. J. F. Ohren *et al.* "Structures of human MAP kinase kinase 1 (MEK1) and MEK2 describe novel noncompetitive kinase inhibition", *Nat Struct Mol Biol* **11**, 1192 (2004).10.1038/nsmb859
16. M. Schroder *et al.* "Catalytic Domain Plasticity of MKK7 Reveals Structural Mechanisms of Allosteric Activation and Diverse Targeting Opportunities", *Cell Chem Biol* **27**, 1285 (2020).10.1016/j.chembiol.2020.07.014
17. Á. Garai *et al.* "Specificity of Linear Motifs That Bind to a Common Mitogen-Activated Protein Kinase Docking Groove", *Science Signaling* **5**, ra74 (2012).doi:10.1126/scisignal.2003004
18. T. Tanoue, M. Adachi, T. Moriguchi, E. Nishida. "A conserved docking motif in MAP kinases common to substrates, activators and regulators", *Nature Cell Biology* **2**, 110 (2000).10.1038/35000065
19. W. Peti, R. Page. "Molecular basis of MAP kinase regulation", *Protein Science* **22**, 1698 (2013).https://doi.org/10.1002/pro.2374
20. A. Zeke *et al.* "Systematic discovery of linear binding motifs targeting an ancient protein interaction surface on MAP kinases", *Mol Syst Biol* **11**, 837 (2015).10.15252/msb.20156269
21. T. Zhou, L. Sun, J. Humphreys, E. J. Goldsmith. "Docking interactions induce exposure of activation loop in the MAP kinase ERK2", *Structure* **14**, 1011 (2006).10.1016/j.str.2006.04.006
22. C. I. Chang, B. E. Xu, R. Akella, M. H. Cobb, E. J. Goldsmith. "Crystal structures of MAP kinase p38 complexed to the docking sites on its nuclear substrate MEF2A and activator MKK3b", *Mol Cell* **9**, 1241 (2002).10.1016/s1097-2765(02)00525-7
23. M. Dyla, M. Kjaergaard. "Intrinsically disordered linkers control tethered kinases via effective concentration", *Proc Natl Acad Sci U S A* **117**, 21413 (2020).10.1073/pnas.2006382117
24. J. Beenstock, N. Mooshayef, D. Engelberg. "How Do Protein Kinases Take a Selfie (Autophosphorylate)?", *Trends in Biochemical Sciences* **41**, 938 (2016).10.1016/j.tibs.2016.08.006
25. E. Park *et al.* "Architecture of autoinhibited and active BRAF-MEK1-14-3-3 complexes", *Nature* **575**, 545 (2019).10.1038/s41586-019-1660-y
26. Y. Kondo *et al.* "Cryo-EM structure of a dimeric B-Raf:14-3-3 complex reveals asymmetry in the active sites of B-Raf kinases", *Science* **366**, 109 (2019).10.1126/science.aay0543
27. D. F. Brennan *et al.* "A Raf-induced allosteric transition of KSR stimulates phosphorylation of MEK", *Nature* **472**, 366 (2011).10.1038/nature09860

28. P. Sok *et al.* "MAP Kinase-Mediated Activation of RSK1 and MK2 Substrate Kinases", *Structure* **28**, 1101 (2020).https://doi.org/10.1016/j.str.2020.06.007
29. E. t. Haar, P. Prabakhar, X. Liu, C. Lepre. "Crystal Structure of the P38α-MAPKAP Kinase 2 Heterodimer*", *Journal of Biological Chemistry* **282**, 9733 (2007).https://doi.org/10.1074/jbc.M611165200
30. L. Braun *et al.* "A Toxoplasma dense granule protein, GRA24, modulates the early immune response to infection by promoting a direct and sustained host p38 MAPK activation", *J Exp Med* **210**, 2071 (2013).10.1084/jem.20130103
31. E. Pellegrini *et al.* "Structural Basis for the Subversion of MAP Kinase Signaling by an Intrinsically Disordered Parasite Secreted Agonist", *Structure* **25**, 16 (2017).10.1016/j.str.2016.10.011
32. T. Bepler *et al.* "Positive-unlabeled convolutional neural networks for particle picking in cryo-electron micrographs", *Nat Methods* **16**, 1153 (2019).10.1038/s41592-019-0575-8
33. V. Modi, R. L. Dunbrack, Jr. "Defining a new nomenclature for the structures of active and inactive kinases", *Proc Natl Acad Sci U S A* **116**, 6818 (2019).10.1073/pnas.1814279116
34. R. Evans *et al.* "Protein complex prediction with AlphaFold-Multimer", *bioRxiv*, 2021.10.04.463034 (2022).10.1101/2021.10.04.463034
35. R. Diskin, D. Engelberg, O. Livnah. "A novel lipid binding site formed by the MAP kinase insert in p38 alpha", *J Mol Biol* **375**, 70 (2008).10.1016/j.jmb.2007.09.002
36. N. Tzarum, Y. Eisenberg-Domovich, J. J. Gills, P. A. Dennis, O. Livnah. "Lipid molecules induce p38alpha activation via a novel molecular switch", *J Mol Biol* **424**, 339 (2012).10.1016/j.jmb.2012.10.007
37. M. Buhrmann, J. Hardick, J. Weisner, L. Quambusch, D. Rauh. "Covalent Lipid Pocket Ligands Targeting p38alpha MAPK Mutants", *Angew Chem Int Ed Engl* **56**, 13232 (2017).10.1002/anie.201706345
38. M. Buhrmann *et al.* "Structure-based design, synthesis and crystallization of 2-arylquinazolines as lipid pocket ligands of p38alpha MAPK", *PLoS One* **12**, e0184627 (2017).10.1371/journal.pone.0184627
39. K. M. Comess *et al.* "Discovery and characterization of non-ATP site inhibitors of the mitogen activated protein (MAP) kinases", *ACS Chem Biol* **6**, 234 (2011).10.1021/cb1002619
40. O. Laufkotter, H. Hu, F. Miljkovic, J. Bajorath. "Structure- and Similarity-Based Survey of Allosteric Kinase Inhibitors, Activators, and Closely Related Compounds", *J Med Chem* **65**, 922 (2022).10.1021/acs.jmedchem.0c02076
41. X. H. Zhang *et al.* "Targeting the non-ATP-binding pocket of the MAP kinase p38γ mediates a novel mechanism of cytotoxicity in cutaneous T-cell lymphoma (CTCL)", *FEBS Letters* **595**, 2570 (2021).https://doi.org/10.1002/1873-3468.14186
42. K. Kirsch *et al.* "Co-regulation of the transcription controlling ATF2 phosphoswitch by JNK and p38", *Nat Commun* **11**, 5769 (2020).10.1038/s41467-020-19582-3
43. X. Liu *et al.* "A conserved motif in JNK/p38-specific MAPK phosphatases as a determinant for JNK1 recognition and inactivation", *Nat Commun* **7**, 10879 (2016).10.1038/ncomms10879
44. E. I. James, T. A. Murphree, C. Vorauer, J. R. Engen, M. Guttman. "Advances in Hydrogen/Deuterium Exchange Mass Spectrometry and the Pursuit of Challenging Biological Systems", *Chem Rev* **122**, 7562 (2022).10.1021/acs.chemrev.1c00279
45. S. A. Foster *et al.* "Activation Mechanism of Oncogenic Deletion Mutations in BRAF, EGFR, and HER2", *Cancer Cell* **29**, 477 (2016).https://doi.org/10.1016/j.ccell.2016.02.010
46. B. Zhang *et al.* "Oncogenic mutations within the β3-αC loop of EGFR/ERBB2/BRAF/MAP2K1 predict response to therapies", *Mol Genet Genomic Med* **8**, e1395 (2020).10.1002/mgg3.1395
47. A. Perez-Gallegos, M. Garcia-Viloca, A. Gonzalez-Lafont, J. M. Lluch. "A QM/MM study of Kemptide phosphorylation catalyzed by protein kinase A. The role of Asp166 as a general acid/base catalyst", *Phys Chem Chem Phys* **17**, 3497 (2015).10.1039/c4cp03579h

48. A. Kuzmanic *et al.* "Changes in the free-energy landscape of p38alpha MAP kinase through its canonical activation and binding events as studied by enhanced molecular dynamics simulations", *Elife* **6** (2017).10.7554/eLife.22175
49. S. Doerr, G. De Fabritiis. "On-the-Fly Learning and Sampling of Ligand Binding by High-Throughput Molecular Simulations", *J Chem Theory Comput* **10**, 2064 (2014).10.1021/ct400919u
50. N. Plattner, S. Doerr, G. De Fabritiis, F. Noe. "Complete protein-protein association kinetics in atomic detail revealed by molecular dynamics simulations and Markov modelling", *Nat Chem* **9**, 1005 (2017).10.1038/nchem.2785
51. F. Pesce, K. Lindorff-Larsen. "Refining conformational ensembles of flexible proteins against small-angle x-ray scattering data", *Biophys J* **120**, 5124 (2021).10.1016/j.bpj.2021.10.003
52. A. H. Larsen *et al.* "Combining molecular dynamics simulations with small-angle X-ray and neutron scattering data to study multi-domain proteins in solution", *PLoS Comput Biol* **16**, e1007870 (2020).10.1371/journal.pcbi.1007870
53. S. Orioli, A. H. Larsen, S. Bottaro, K. Lindorff-Larsen. "How to learn from inconsistencies: Integrating molecular simulations with experimental data", *Prog Mol Biol Transl Sci* **170**, 123 (2020).10.1016/bs.pmbts.2019.12.006
54. N. S. González-Foutel *et al.* "Conformational buffering underlies functional selection in intrinsically disordered protein regions", *Nature Structural & Molecular Biology* **29**, 781 (2022).10.1038/s41594-022-00811-w
55. Y. FLEMING *et al.* "Synergistic activation of stress-activated protein kinase 1/c-Jun N-terminal kinase (SAPK1/JNK) isoforms by mitogen-activated protein kinase kinase 4 (MKK4) and MKK7", *Biochemical Journal* **352**, 145 (2000).10.1042/bj3520145
56. C. Tournier, A. J. Whitmarsh, J. Cavanagh, T. Barrett, R. J. Davis. "The MKK7 Gene Encodes a Group of c-Jun NH₂-Terminal Kinase Kinases", *Molecular and Cellular Biology* **19**, 1569 (1999).doi:10.1128/MCB.19.2.1569
57. T. O. Fischmann *et al.* "Crystal structures of MEK1 binary and ternary complexes with nucleotides and inhibitors", *Biochemistry* **48**, 2661 (2009).10.1021/bi801898e
58. V. Modi, R. L. Dunbrack. "A Structurally-Validated Multiple Sequence Alignment of 497 Human Protein Kinase Domains", *Scientific Reports* **9**, 19790 (2019).10.1038/s41598-019-56499-4
59. Y. Y. Zhang, J. W. Wu, Z. X. Wang. "A distinct interaction mode revealed by the crystal structure of the kinase p38α with the MAPK binding domain of the phosphatase MKP5", *Sci Signal* **4**, ra88 (2011).10.1126/scisignal.2002241
60. C. Dominguez, D. A. Powers, N. Tamayo. "p38 MAP kinase inhibitors: many are made, but few are chosen", *Curr Opin Drug Discov Devel* **8**, 421 (2005)
61. Y. L. Wang *et al.* "Kinetic and mechanistic studies of p38alpha MAP kinase phosphorylation by MKK6", *FEBS J* **286**, 1030 (2019).10.1111/febs.14762
62. J. M. Humphreys, A. T. Piala, R. Akella, H. He, E. J. Goldsmith. "Precisely Ordered Phosphorylation Reactions in the p38 Mitogen-activated Protein (MAP) Kinase Cascade*", *Journal of Biological Chemistry* **288**, 23322 (2013).https://doi.org/10.1074/jbc.M113.462101
63. K. Aoki, K. Takahashi, K. Kaizu, M. Matsuda. "A Quantitative Model of ERK MAP Kinase Phosphorylation in Crowded Media", *Scientific Reports* **3**, 1541 (2013).10.1038/srep01541
64. C. Salazar, T. Höfer. "Multisite protein phosphorylation – from molecular mechanisms to kinetic models", *The FEBS Journal* **276**, 3177 (2009).https://doi.org/10.1111/j.1742-4658.2009.07027.x
65. https://doi.org/10.26037/yareta:5w7luymjcncd3ipjm3v76bqezm

Acknowledgments:

PJ was supported by a EMBL predoctoral fellowship. We thank Stephen Cusack and Andrew McCarthy (EMBL Grenoble) for encouragement, Wojtek Galej (EMBL Grenoble) for critical reading of the manuscript and Mohamed-Ali Hakimi (IAB, Grenoble) for introducing us to the *T. gondii* protein GRA24. We acknowledge Sarah Schneider for her support in using the EM Facility at EMBL Grenoble and thank Felix Weiss, Wim Hagen and Simon Fromm for excellent data collection at the EMBL Imaging Centre. We thank Alice Aubert (EMBL, Grenoble) for support in eukaryotic protein expression, the proteomic core facility at EMBL Heidelberg for mass spectrometry and Ulrike Kapp (ESRF) for assistance in the crystallisation of p38α. We acknowledge Massimiliano Bonomi (Institut Pasteur - CNRS, France) for discussions and technical support in cross-correlation analysis. Kresten Lindorff-Larsen, Sandro Bottaro and Francesco Pesce are acknowledged for support in running the BME procedure. This work used the platforms of the Grenoble Instruct-ERIC centre (ISBG ; UAR 3518 CNRS-CEA-UGA-EMBL) within the Grenoble Partnership for Structural Biology (PSB), supported by FRISBI (ANR-10-INBS-0005-02) and GRAL, financed within the University Grenoble Alpes graduate school (Ecoles Universitaires de Recherche) CBH-EUR-GS (ANR-17-EURE-0003). We acknowledge the European Synchrotron Radiation Facility for the provision of synchrotron radiation facilities, and we would like to thank the staff of the ESRF and EMBL Grenoble for assistance and support in using beamlines ID23-1 and ID23-2. SAXS data were collected at beamline B21 at Diamond Light Source, UK. Molecular graphics and analyses were performed with UCSF ChimeraX, developed by the Resource for Biocomputing, Visualization, and Informatics at the University of California, San Francisco, with support from National Institutes of Health R01-GM129325 and the Office of Cyber Infrastructure and Computational Biology, National Institute of Allergy and Infectious Diseases. We acknowledge PRACE and the Swiss National Supercomputing Centre (CSCS) for large supercomputer time allocations on Piz Daint, project IDs: pr126, s1107.

Funding:

EMBL (MWB)

Swiss National Science Foundation [projects number: 200021_204795] (FLG).

Bridge [40B2-0_203628] (FLG).

Author contributions:

Conceptualization: PJ, EP, FLG and MWB

Methodology: PJ, IG, DG, JvV, MP and OV

Investigation: PJ, IG, DG, JvV, OV, MT, FLG, EP, and MWB

Visualization: PJ, IG, DG, JvV and OV

Funding acquisition: FLG and MWB

Supervision: FLG, EP and MWB

Writing - original draft– PJ and MWB

Writing – review & editing: PJ, IG, DG, JvV, MP, OV, MT, FLG, EP, and MWB

Competing interests: Authors declare that they have no competing interests.

Data and materials availability:

Accession codes: Structure of the MKK6^{DD}GRA-p38α^{T180V} complex: EMPIAR-11203 (raw micrographs; Electron Microscopy Public Image Archive), EMD-15233 (map; Electron Microscopy Data Bank) and PDB-8A8M (coordinates; Protein Data Bank). Crystal structures of apo p38α and p38α^{K53R}: PDB-5ETC and PDB-5ETI (coordinates and structure factors; Protein Data Bank). The SAXS curves and pair distribution functions are deposited in the Small Angle Scattering Biological Data Bank (access codes: SASBDB-SASDRC6 and SASBDB-SASDRD6). The mass spectrometry proteomics data have been deposited to the ProteomeXchange Consortium via the PRIDE partner repository with the dataset identifier PXD040499 and 10.6019/PXD040499. The MD simulations data (trajectories, topology files, and structures of the SAXS-refined ensembles) are deposited in the YARETA repository *(65)*.

Supplementary Materials

Supplementary Materials and Methods

Supplementary Text

Figs. S1 to S16

Tables S1 to S10

References (*64–116*)

Movies S1 to S16

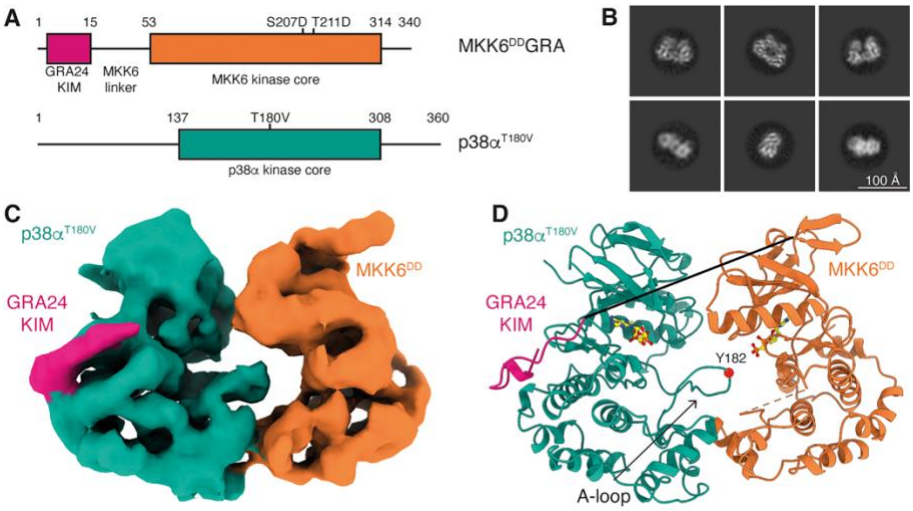

Fig. 1. Structure of the MKK6^{DD}GRA-p38α^{T180V} complex. (**A**) Schematic of the two protein constructs. Key domains and mutations are indicated. (**B**) Representative 2D class averages from single-particle cryo-EM analysis of the MKK6^{DD}GRA-p38α^{T180V} complex. (**C**) Segmented single-particle reconstruction cryo-EM map of the MKK6^{DD}GRA-p38α^{T180V} complex, resolved to 4 Å resolution and coloured according to (A). (**D**) Model of the MKK6^{DD}GRA-p38α^{T180V} complex showing the overall structure of the complex. MKK6^{DD}GRA-p38α^{T180V} is represented as a cartoon and coloured according to (A), AMP-CP nucleotides are represented as balls and sticks (carbon atoms yellow). The MKK6 linker and A-loop are disordered and respectively shown as a full black line and an orange dashed line. The position of the Y182 residue in the p38α A-loop is indicated by a red sphere.

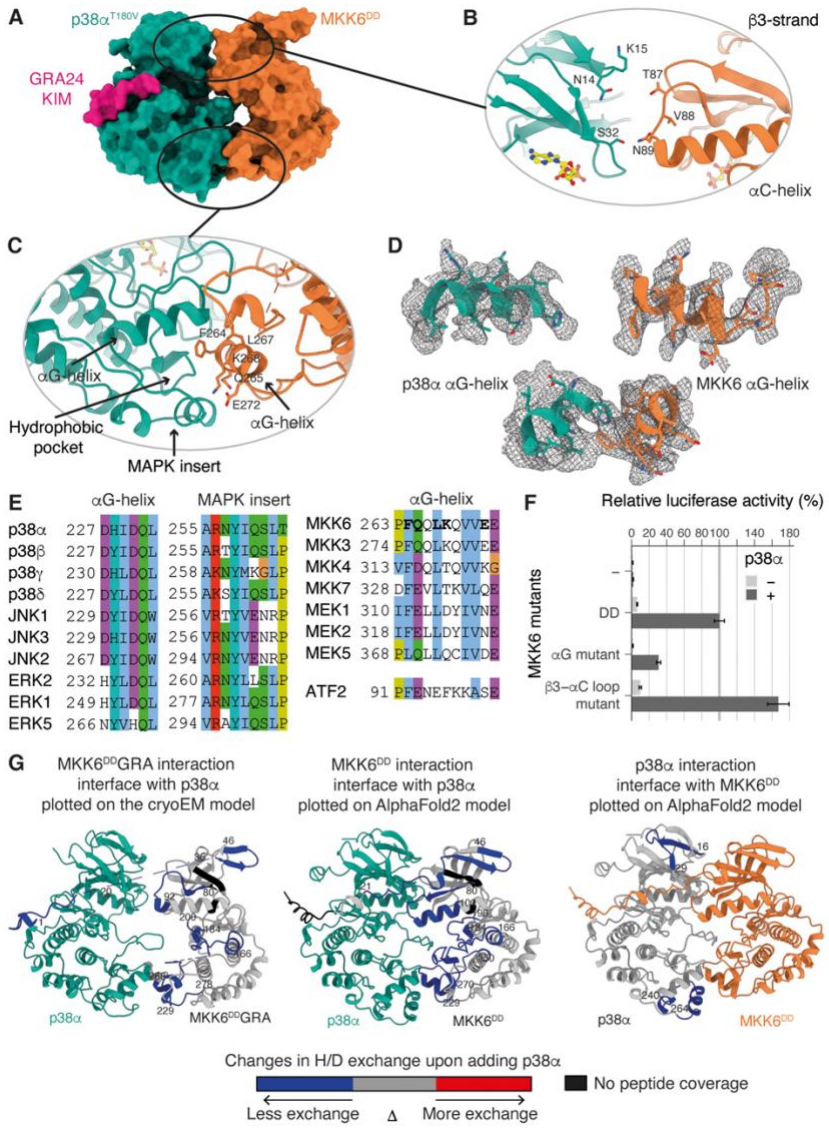

Fig. 2. Interaction interfaces between MKK6 and p38α, distal from the active site. (**A**) Surface representation of the MKK6^{DD}GRA-p38α^{T180V} complex. (**B**) Potential interaction between the N-lobes. (**C**) Interaction between the αG-helix of MKK6 and the hydrophobic pocket of p38α. (**D**) αG-helices of p38α and MKK6 in the sharpened Coulomb potential map (black mesh). (**E**) Sequence alignment of MAPK hydrophobic pockets, MAP2K αG-helices and the p38α substrate ATF2 peptide (Clustal colouring scheme). (**F**) Luciferase reporter assay to monitor the activity of the p38α signalling pathway in HEK293T cells, showing the ability of MKK6^{DD} mutants to activate p38α (statistical analysis in Table S6 and protein expression levels in Fig. S10). (**G**) MKK6^{DD}GRA (left) and MKK6^{DD} (middle) interaction sites with p38α, and p38α interaction sites with MKK6^{DD}(right), identified by HDX-MS. Regions showing protection upon the addition of p38α or MKK6^{DD}, indicative of interaction, are highlighted in blue.

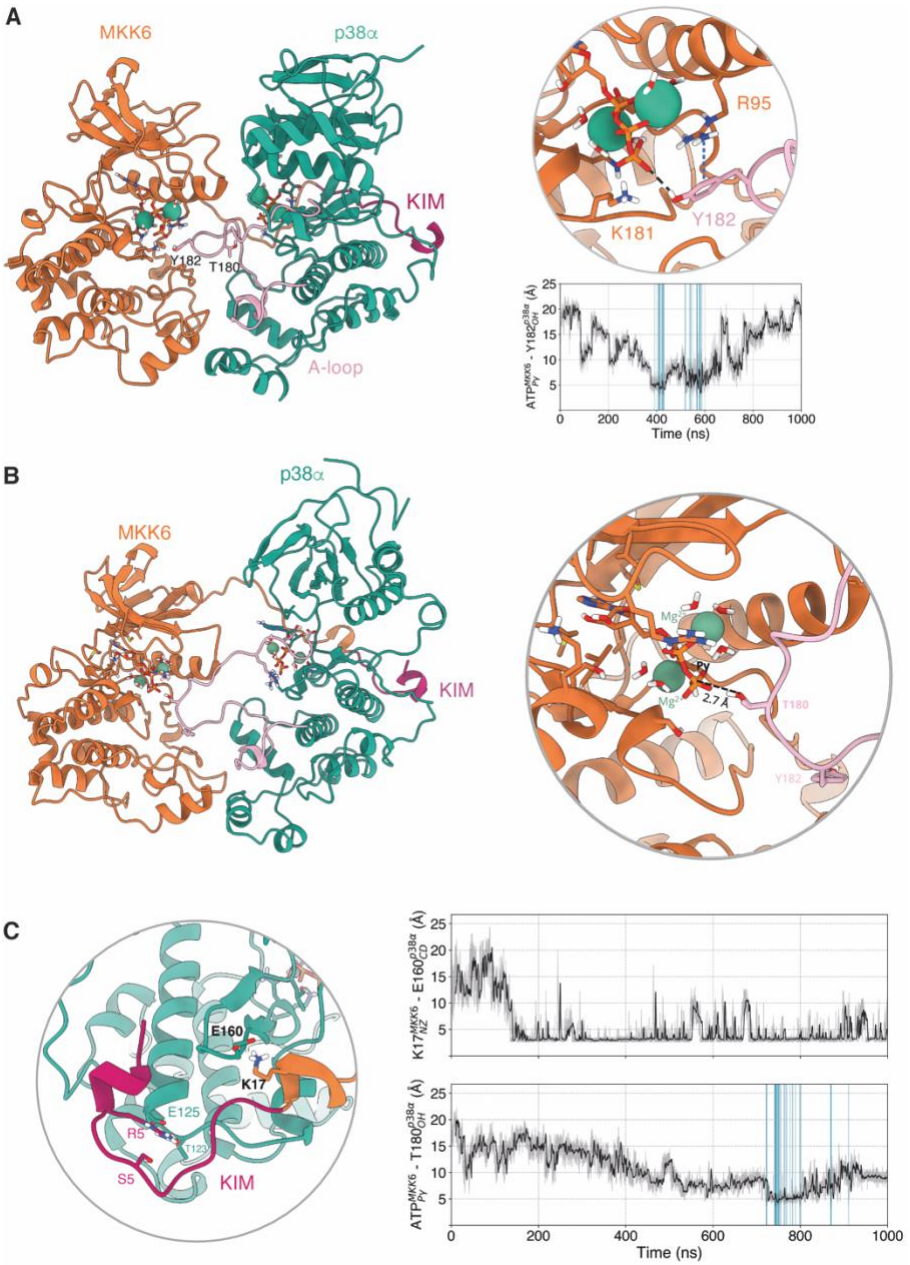

Fig. 3. MD simulations show that both p38α Y182 and T180 can approach MKK6 ATP and that a rotated conformation of p38α favours T180 phosphorylation. (**A**) Frame extracted from one of the unrestrained MD simulations in which Y182 approaches the γ-phosphate of MKK6 ATP at a catalytically compatible distance (3.8 Å). The π-cation interaction of R95 with Y182 that further stabilizes Y182 close to ATP is shown in a blue dashed line. The frames where p38α Y182 reaches MKK6 ATP at a catalytically compatible distance in this set of simulations are highlighted in the plot of distances over time (blue). (**B**) Simulation frame in which p38α has rotated around its axis with respect to the cryo-EM structure. (**C**) Detailed view around the KIM. The frames where T180 reaches MKK6 ATP at a catalytically compatible distance in this set of simulations are highlighted in the plot of distances over time (blue).

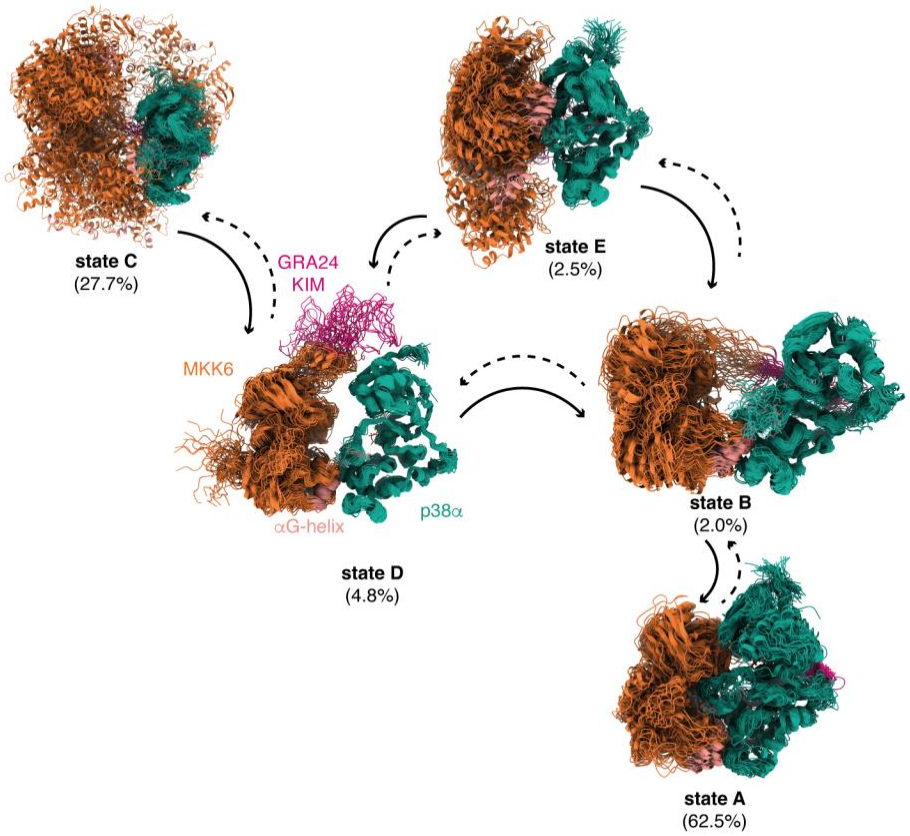

Fig. 4. Kinetic-based clustering of the accumulated simulations of MKK6GRA-p38α. Each macro-state shows an overlay of 50 representative conformations sampled proportionally to the equilibrium probability of each micro-state in the corresponding macro-state corresponding to different kinetically distinct states. The population of each state as derived from the fitting to the $MKK6^{DD}GRA + p38\alpha^{WT} + ADP + AlF_4^-$ SAXS curve (Fig. S2) is given in parenthesis.

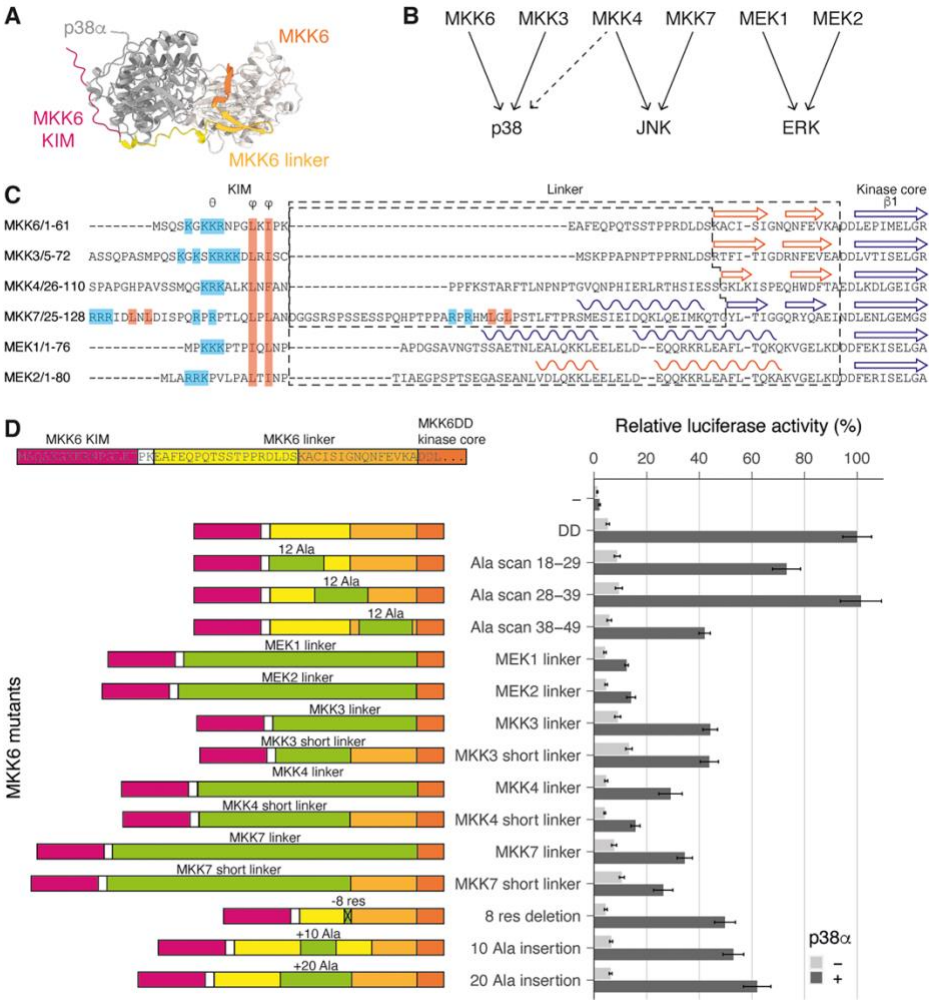

Fig. 5. MKK6 N-terminal extension length and secondary structure define the specificity of p38α activation. (**A**) Top view of an MKK6-p38α AlphaFold2 multimer model, for illustrative purposes. (**B**) Specificity of the MAP2K/MAPK signalling pathways. (**C**) Sequence alignment of MAP2K N-termini. Secondary structure elements are indicated, from experimental structures in blue and AlphaFold2 predictions (pLDDT score > 65) in orange. (**D**) Luciferase reporter assay to monitor the activity of the p38α signalling pathway in HEK293T cells showing the ability of $MKK6^{DD}$ mutants and chimeras to activate p38α (statistical analysis in Table S10 and protein expression levels in Fig. S10).